Total-Field/Scattered-Field Separation Based on *H*-field Correction for the 3-D Nonstandard Finite-Difference Time-Domain Method

Tadao Ohtani[1], Yasushi Kanai[2], and Nikolaos V. Kantartzis[3]

[1]1-17-134 Omachi, Asahikawa 070-0841, Japan, bytcg100@ybb.ne.jp
[2]Niigata Institute of Technology, Kashiwazaki 945-1195, Japan, kanai@iee.niit.ac.jp
[3]Aristotle University of Thessaloniki, GR-54124 Thessaloniki, Greece, kant@auth.gr

The nonstandard finite-difference time-domain (NS-FDTD) methodology is a very competent numerical tool for the radar cross section (RCS) analysis of scattering objects with complicated geometries and electrically large sizes, due to its high accuracy at fixed frequencies. During the RCS calculation via the typical FDTD scheme, the total-field/scattered-field (TF/SF) approach is generally used to separate the SF from TF simulation region. However, current TF/SF separation algorithms for the NS-FDTD method are rather laborious for practical arrangements. Therefore, we develop a new TF/SF separation technique, solely based on *H*-field correction, and apply it in both cubic- and rectangular-cell computational domains, which discretize demanding structures. In all scenarios, the proposed algorithm is found to be superior over previously-derived procedures, while, concurrently, remaining much simpler in its overall NS-FDTD implementation.

***Index Terms*—Dispersion errors, FDTD methods, nonstandard forms, radar cross section analysis, scattering.**

I. Introduction

The nonstandard finite-difference time-domain (NS-FDTD) technique constitutes an advanced rendition of the FDTD method [1]. Incorporating a robust error compensation concept along the propagation direction in the NS scheme and Yee's cell space, it achieves impressive levels of isotropy and accuracy at specific frequencies; around 4 magnitude orders higher than its usual FDTD counterpart [2]. So, it can be deemed suitable for the scattering analysis of electrically large objects, like the radar cross section (RCS) extraction of aircrafts with complex shape. For the prior RCS, the scattered field (SF) must be derived from the total field (TF) in the computational domain. To this aim, the TF/SF formulation has been combined with the FDTD approach [2]. However, the existing TF/SF separation scheme for the NS-FDTD method [3] is somewhat complicated for practical use.

Regarding this issue, a novel TF/SF concept, based only on ***H***-field correction, is proposed in the paper. It is, numerically, proven that our technique overwhelms previous ones [3], while being much simpler. It is emphasized that the featured TF/SF scheme is equivalently applicable to both cubic and rectangular cells. Results substantiate the superior accuracy, stability, and consistency of the developed algorithm in the RCS assessment of real-world structures by means of the 3-D NS-FDTD method.

II. TF/SF Scheme Based on *H*-Field Correction

Current TF/SF separation schemes, basically, focus on ***E***-field correction [3]. In contrast, herein, the proposed method stems TF/SF formulation stems only from the ***H***-field correction. The calculation flow is shown in Fig. 1, where n is the time step, $j^2 = -1$, ω the angular frequency, Δt the time increment, $\boldsymbol{k}_{\text{num}}$ the numerical wavevector [4], $\boldsymbol{r}$ the position vector, $\boldsymbol{H}_0$ the magnetic field amplitude, and $(\boldsymbol{E}, \boldsymbol{H})_{\text{sub}}$ terms calculated separately from the main NS-FDTD calculation. Moreover, $\nabla^{(0)}$ and $\nabla^{(1)}$ are the Hamilton operators in the NS-FDTD method [4], $S_\omega(\Delta t) = 2\sin(\omega\Delta t/2)/\omega$ and $\bar{\nu}$ a tuning parameter for field matching, evaluated numerically in advance. On the other hand, the area structure and the calculation procedure are illustrated in Fig. 2.

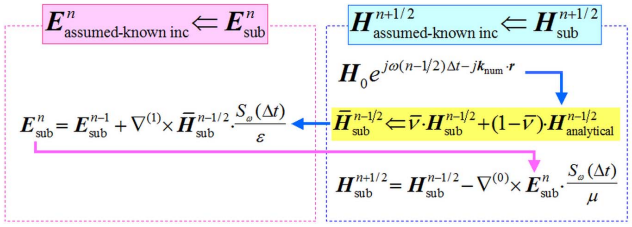

Fig. 1. Calculation flow chart for $(\boldsymbol{E},\boldsymbol{H})_{\text{assumed-known inc}}$ terms, based on ***H***-field correction, using $0 \le \bar{\nu} \le 1$.

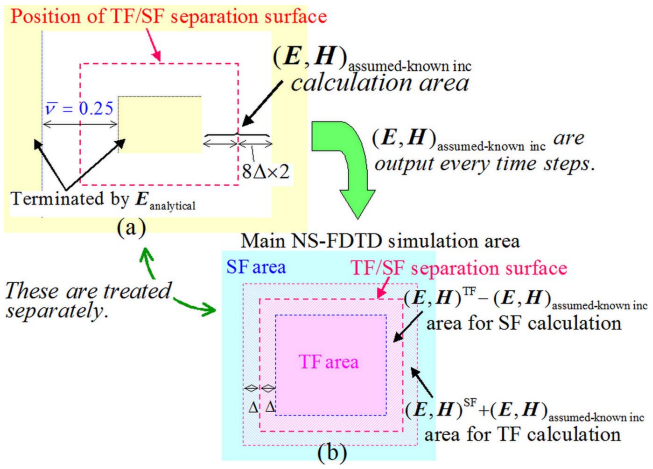

Fig. 2. (a) Structural setup for the calculation of the $(\boldsymbol{E}, \boldsymbol{H})_{\text{assumed-known inc}}$ terms. (b) The TF/SF separation process applied around the TF/SF separation surface in the main NS-FDTD simulation area.

Note that $\nabla^{(0)}$ spreads over 3 cells and thus, we adopt an 8Δ-wide computation region for the $(\boldsymbol{E}, \boldsymbol{H})_{\text{assumed-known inc}}$ terms on both sides of the TF/SF separation surface to include the 3-cell width. These areas are truncated by $\boldsymbol{E}_{\text{analytical}}$ fields, as depicted in Fig. 2(a). Compared to regular versions [3], the proposed $(\boldsymbol{E}, \boldsymbol{H})_{\text{assumed-known inc}}$ calculation procedure is much easier, since it does not require a correction for the $\boldsymbol{E}_{\text{sub}}$ fields and a multi-layered area, as, also, detected in Figs 1 and 2(a). In this way, the new concept enables the efficient and stable utilization of the TF/SF separation model in the 3-D NS-FDTD technique.

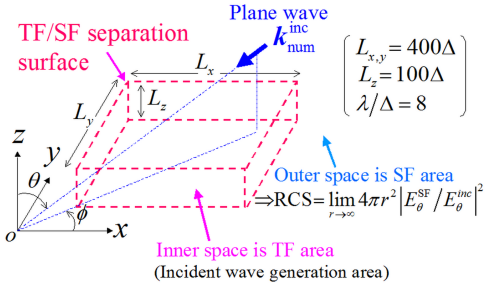

Fig. 3. A straightforward model to determine $\bar{\nu}$ in the free space.

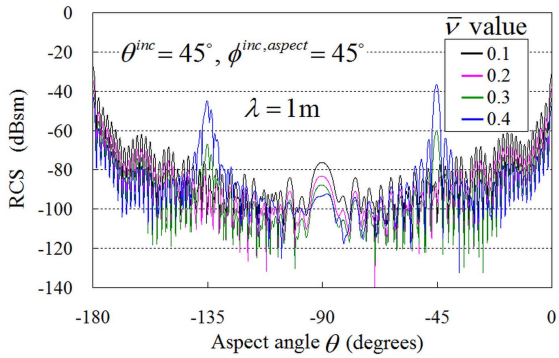

Fig. 4. RCS generated from the TF/SF separation surface without a scatterer.

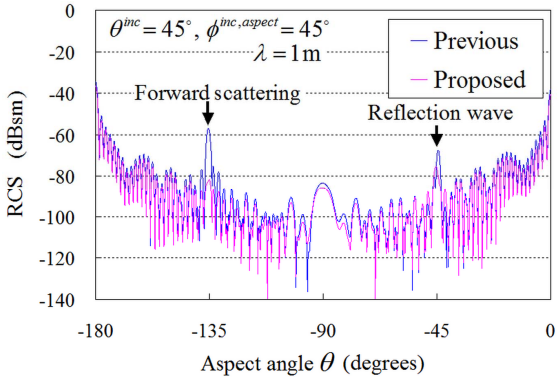

Fig. 5. RCS comparison between existing schemes and the proposed technique, through the calculation model of Fig. 3. The featured formulation is proven to be significantly more effective in the treatment of forward and reflection directions.

III. Numerical Results and Discussion

For the certification of our scheme, we investigate the artificial waves, emanating from the TF/SF separation surface to the outer space. Then, the featured technique is verified by means of RCS values, extracted from the near-to-far-field transformation [2] of the field components located at the SF.

A. Determination of $\bar{\nu}$ and the TF/SF separation performance

An instructive model to obtain the optimum $\bar{\nu}$ is described in Fig. 3. The SF is generated by an incident plane wave in the TF area, while Fig. 4 gives the results for the TF/SF separation surface, without any scatterers in the TF region. For the domain lattice, we select cubic cells of side Δ and $\bar{\nu}$ varies from 0.1 to 0.4. As observed, unphysical SF arises both along the forward and reflection direction for $\bar{\nu} > 0.3$, which increases constantly for $\bar{\nu} < 0.2$, indicating that the 0.2-0.3 values can be a suitable choice for $\bar{\nu}$. Furthermore, by properly adjusting $\bar{\nu}$ we obtain the $(\theta,\phi)^{aspect}$ cases of Fig. 5, which prove that our method, on the whole, leads to smaller RCS outcomes when compared to current approaches [3]. So, it is deduced that the performance of the proposed TF/SF formulation is significantly enhanced.

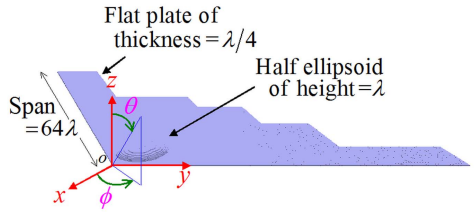

Fig. 6. The discretized model of a B2 aircraft by means of orthogonal cells. Note that the cockpit is modeled in terms of a half ellipsoid.

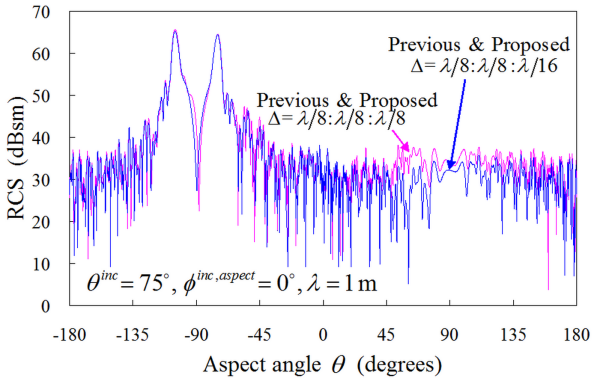

Fig. 7. RCS calculation of the B2 model for $\bar{\nu} = 0.25$. The discrepancies between the two formulations are hardly visible on the plots.

B. RCS analysis of a B2 Spirit aircraft

Next, we proceed to the RCS analysis of the more complex B2 Spirit aircraft. Since its geometry and composition are not fully disclosed, the structure has been discretized to optimally approximate the realistic model of [5]. To this requirement, we have chosen orthogonal cells of perfect electric conductor with $\Delta_{x,y} = \lambda/8$ and $\Delta_z = \lambda/8$, $\lambda/16$, as displayed in Fig. 6. Specifically, the total cell number is 2,156,800 for $\Delta_z = \lambda/8$ and 3,349,352 for $\Delta_z = \lambda/16$. This model is, then, incorporated in the TF/SF separation area (Fig. 3), with $L_x = 490\Delta_x$, $L_y = 696\Delta_y$, and $L_z = 40\Delta_z$. In this context, Fig. 7 presents the RCS results compared to those of [3] (reference). It is detected that both schemes are in very good agreement, revealing their equivalently sufficient TF/SF separation behavior. Additionally, the featured concept is adequately capable in the case of non-cubic cells, despite the simplicity of the algorithm, explained in Figs. 1 and 2. So, the high accuracy and straightforward realization are the two key assets of our formulation. These merits can be very useful for the RCS calculation of various aircrafts, with electrically large sizes and complicated shapes, via the NS-FDTD method.

References

[1] J. B. Cole, "High-accuracy Yee algorithm based on nonstandard finite differences: New developments and verifications," *IEEE Trans. Antennas Propag.*, vol. 50, no. 9, pp. 1185–1191, Sep. 2002.

[2] A. Taflove and S. Hagness, *Computational Electrodynamics: The Finite-Difference Time-Domain Method*. Norwood, MA: Artech House, 2005.

[3] T. Ohtani, Y. Kanai, and N. V. Kantartzis, "Wide-angle elimination of TF/SF-generated spurious waves in the nonstandard FDTD method," *IEEE Trans. Magn.*, 2016 (submitted).

[4] T. Ohtani and Y. Kanai, "Coefficients of finite difference operator for rectangular cell NS-FDTD method," *IEEE Trans. Antennas Propag.*, vol. 59, no. 1, pp. 206–213, Jan. 2011.

[5] https://en.wikipedia.org/wiki/Northrop_Grumman_B-2_Spirit.